CHAPTER 15

High-Carbon Steels: Fully Pearlitic Microstructures and Applications

Introduction

THE TRANSFORMATION OF AUSTENITE to pearlite has been described in Chapter 4, "Pearlite, Ferrite, and Cementite," and Chapter 13, "Normalizing, Annealing, and Spheroidizing Treatments; Ferrite/Pearlite Microstructures in Medium-Carbon Steels," which have shown that as microstructure becomes fully pearlitic as steel carbon content approaches the eutectiod composition, around 0.80% carbon, strength increases, but resistance to cleavage fracture decreases. This chapter describes the mechanical properties and demanding applications for which steels with fully pearlitic microstructures are well suited.

With increasing cooling rates in the pearlite continuous cooling transformation range, or with isothermal transformation temperatures approaching the pearlite nose of isothermal transformation diagrams, Fig. 4.3 in Chapter 4, the interlamellar spacing of pearlitic ferrite and cementite becomes very fine. As a result, for most ferrite/pearlite microstructures, the interlamellar spacing is too fine to be resolved in the light microscope, and the pearlite appears uniformly dark. Therefore, to resolve the interlamellar spacing of pearlite, scanning electron microscopy, and for the finest spacings, transmission electron microscopy (TEM), are necessary to resolve the two-phase structure of pearlite. Figure 15.1 is a TEM micrograph showing very fine interlamellar structure in a colony of pearlite from a high-carbon steel rail. This remarkable composite structure of duc-

tile ferrite and high-strength cementite is the base microstructure for rail and the starting microstructure for high-strength wire applications.

Mechanical Properties of Fully Pearlitic Microstructures

The Gladman et al. equation, Eq 13.2, for the strength of ferrite/pearlite steels shows that the interlamellar spacing of ferrite and cementite lamellae in pearlite becomes more important as the amount of pearlite increases (Ref 15.1). Hyzak and Bernstein in a study of fully pearlitic microstructures in a steel containing 0.81% C evaluated not only the effect of pearlite interlamellar spacing, S, but also the effect of austenite grain size, d, and pearlite colony size, P, on mechanical properties (Ref 15.2). Figure 15.2 shows the dependence of hardness and yield strength on pearlite spacing, and the following equation incorporates, in addition to interlamellar spacing, the effects of austenitic grain size and pearlite colony size on yield strength:

$$\text{Yield strength (MPa)} = 2.18(S^{-1/2}) - 0.40(P^{-1/2}) - 2.88(d^{-1/2}) + 52.30 \quad \text{(Eq 15.1)}$$

In view of this work, pearlite interlamellar spacing is confirmed to be the major microstructural parameter that controls strength of pearlitic microstructures.

Resistance to cleavage fracture of fully pearlitic steels is found to be primarily dependent on austenitic grain size according to the following equation (Ref 15.2):

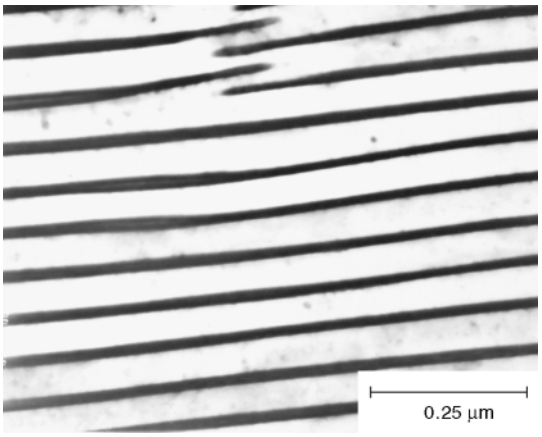

Fig. 15.1 Microstructure of pearlite in rail steel, courtesy of Rocky Mountain Steel Mills, Pueblo, CO. TEM micrograph of thin foil taken by Robert A. McGrew at the Colorado School of Mines

$$\text{Transition temperature (°C)} = -0.83(P^{-1/2}) - 2.98(d^{-1/2}) + 217.84 \quad \text{(Eq 15.2)}$$

This equation shows that the transition temperature for fully pearlitic steels is invariably above room temperature, and fracture around room temperature is therefore characterized by cleavage on {100} planes of the ferrite in pearlite. In another study, the size of cleavage facets was found to be a strong function of, but always smaller than, the austenite grain size and appeared to be related to common ferrite orientations in several adjoining pearlite colonies (Ref 15.3).

Rail Steels: Structure and Performance

The papers of proceedings volumes of several symposia address the ever-increasing demands placed on rail steels and the approaches used to improve rail steel performance (Ref 15.4–Ref 15.6). Rails are subject to heavy contact cyclic loading that accompanies increased car size and loading, to 100 and 125 ton capacity, increased train size, and increased train speeds used to transport bulk products over the last several decades. These increasing demands require manufacturing and metallurgical approaches that offset wear and other types of failure that limit rail life. An early type

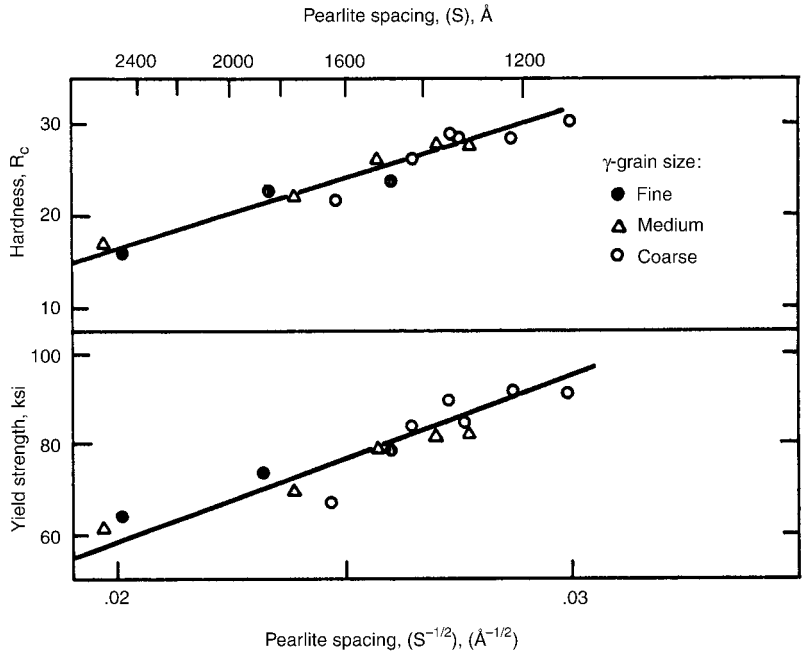

Fig. 15.2 Hardness and yield strength as a function of pearlite interlamellar spacing in fully pearlitic microstructures. From Hyzak and Bernstein, Ref 15.2

of rail failure was associated with entrapped hydrogen that produced *shatter crack or flakes* in heavy rail sections, but that difficulty has been effectively controlled by controlled cooling and by vacuum degassing of liquid steel (Ref 15.5–15.7).

Wear of rail has been studied by laboratory testing and also in a unique facility that subjects rail to actual train service. The latter facility, the Facility for Accelerated Service Testing (FAST), Pueblo, Colo., is a 4.8 mile loop of track on which test trains with 9500 trailing tons have completed up to 120 laps daily in order to evaluate the processing, chemistry, and performance of rails under actual service conditions (Ref 15.8). In a study of rail tested at the FAST facility, wear was found to be a three-stage process (Ref 15.9). The first stage consisted of severe plastic deformation in a thin surface layer of the rail, on the order of 0.1 mm (0.004 in.) in depth, in response to repeated heavy compressive and shear loading produced by the passage of test trains. Two steels were evaluated, and the depth of the deformed zone was shallower in the harder steel. The second stage consisted of the development of subsurface cracks in the severely deformed layer, generally at the interface of the deformed layer and the undeformed microstructure. The propagation of cracks to the surface of the rail and the associated spalling off of small slivers or flakes of the rail constituted the third stage of wear. This sequence of deformation and fracture is repeated many times to produce substantial rail wear. Kapoor has referred to the repeated cycles of compressive deformation as *plastic ratcheting* and notes that cracking serves primarily to create the wear debris (Ref 15.10).

Improved rail wear resistance correlates with fine interlamellar ferrite/cementite spacing of pearlitic microstructures, which, as noted previously,

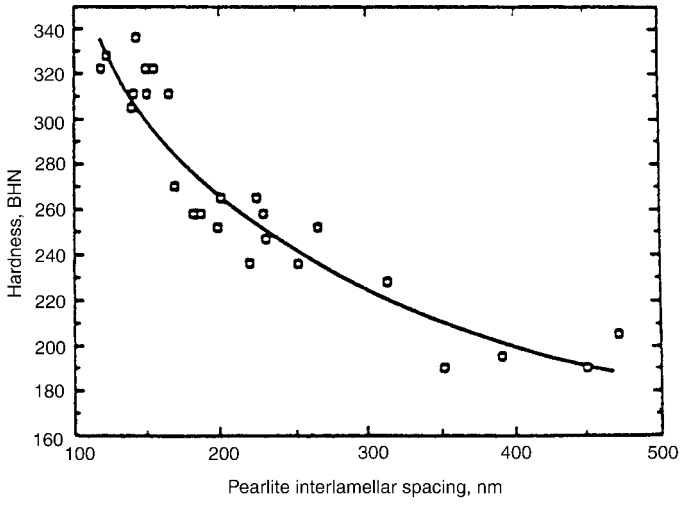

Fig. 15.3 Hardness as a function of pearlite interlamellar spacing for various rail steels. From Clayton and Danks, Ref 15.11

increases hardness and strength. Figure 15.3 shows the hardness correlation with pearlite interlamellar spacing, and Fig. 15.4 and 15.5 show, respectively, that wear decreases with decreasing interlamellar spacing and increasing hardness of pearlitic microstructures in a series of rail steels (Ref 15.11). The latter results were generated by rolling/sliding wear tests in which the maximum Hertzian contact pressure was varied by adjusting the loads applied by test rollers. As shown in Fig. 15.4 and 15.5, increasing contact pressure accelerates wear.

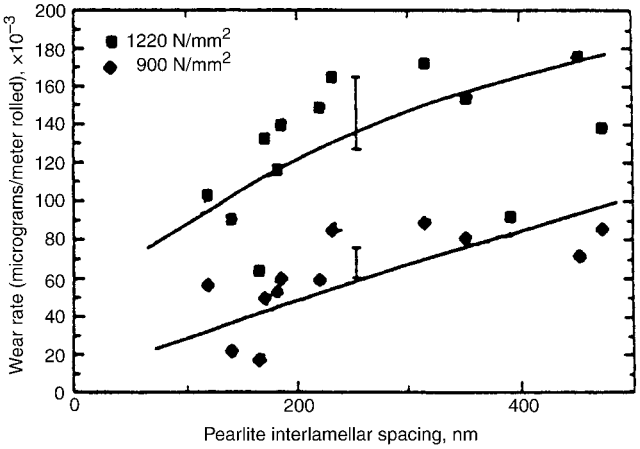

Fig. 15.4 Wear rate as a function of pearlite interlamellar spacing for various rail steels at contact pressures of 1220 N/mm^2 and 900 N/mm^2. From Clayton and Danks, Ref 15.11

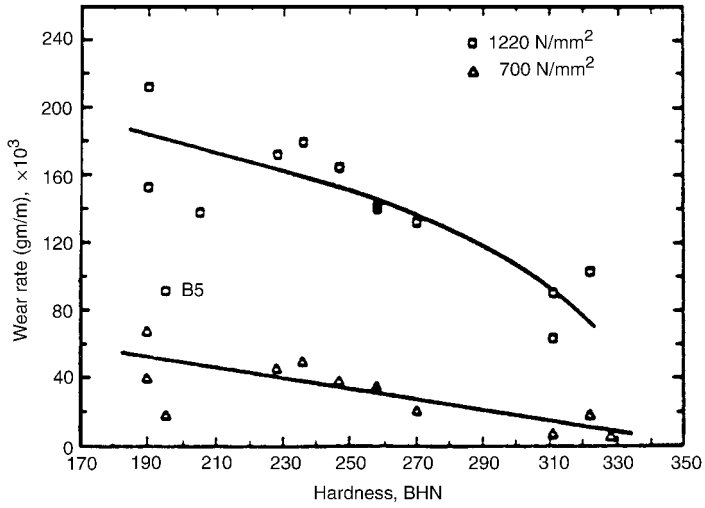

Fig. 15.5 Wear rate as a function of hardness for various rail steels tested at contact pressures of 1220 N/mm^2 and 700 N/mm^2. From Clayton and Danks, Ref 15.11

The strong correlation of improved rail wear resistance with fine pearlite interlamellar spacing and high pearlite hardness has led to processing and alloying approaches to produce fine pearlite. An effective processing approach has been to produce pearlite of fine interlamellar spacing and high hardness on the surface of rails by *head hardening* heat treatments, applied by accelerated cooling with forced air, water sprays, or oil or aqueous polymer quenching either online while the steel is still austenitic immediately after hot rolling or by offline reheating of as-rolled rails (Ref 15.12, 15.13). Figure 15.6 shows the high head hardness of an offline head-hardened rail section (Ref 15.12). Alloying approaches to refine pearlite interlamellar spacing have included alloying with chromium, molybdenum, vanadium, and silicon (Ref 15.14–15.18) and the development of rail steels with hypereutectoid carbon contents (Ref 15.19).

The rolling contact loading of rails eventually creates complex interactions of strain hardening and residual stress distributions that not only influence wear but may also nucleate and propagate cracks transverse to rail lengths. Rails in curves are the most severely stressed portions of track, and Fig. 15.7 shows schematically some of the damage phenomena that may originate in rail curves under heavy traffic conditions (Ref 15.20). Subsurface cracks may also develop. *Detail fracture* is defined as "a transverse fatigue crack progressing from the corner of the rail head" (Ref 15.21), and *shelling* is "a condition where the rail steel, stressed beyond its elastic limit, deforms and fails in subsurface shear" (Ref 15.7). Steele and Joerms have analyzed the stress states associated with shelling (Ref 15.22). Compressive residual stresses develop at the surface of rails and are balanced by interior tensile stresses. Shell cracking initiates in lower hardness regions underneath work-hardened rail surface layers and eventually turns into detail fractures.

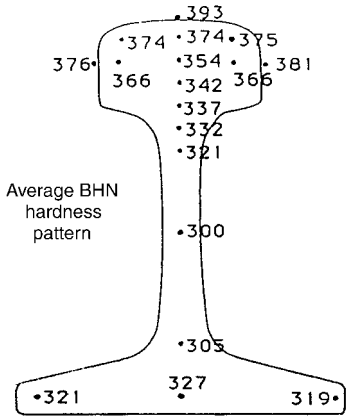

Fig. 15.6 Hardness as a function of location in a transverse section of rail subjected to offline head hardening heat treatment. From George et al., Ref 15.12

Patenting: Pearlite Formation for High-Strength Steel Wire

Pearlitic microstructures in steels of eutectoid composition are drawn to wires that have the highest useable tensile strengths of any steel products. The strengths depend on steel quality, the microstructure prior to wire drawing, and on the amount of wire drawing to produce a finished wire diameter. Figure 15.8 shows tensile strength as a function of wire diameter for hypereutectoid steel wires capable of resisting delamination (Ref 15.23), and Fig. 15.9 shows the tensile strengths of patented and drawn wires from a number of studies (Ref 15.24). Remarkably high strengths, ranging up to almost 6000 MPa (870 ksi), can be produced. High-strength wires are often further incorporated into bunched arrays for

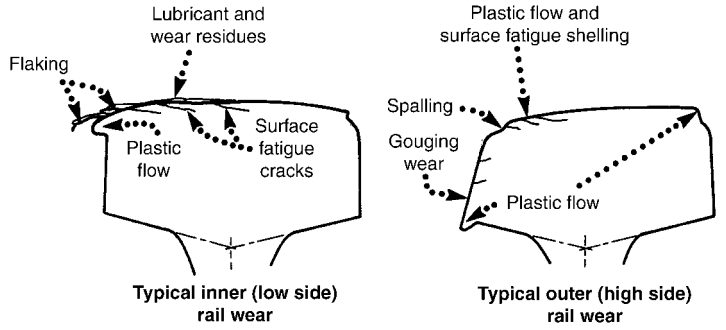

Fig. 15.7 Schematic diagram of wear and damage to curved rails under heavy traffic conditions. From Kalousek and Bethune, Ref 15.20

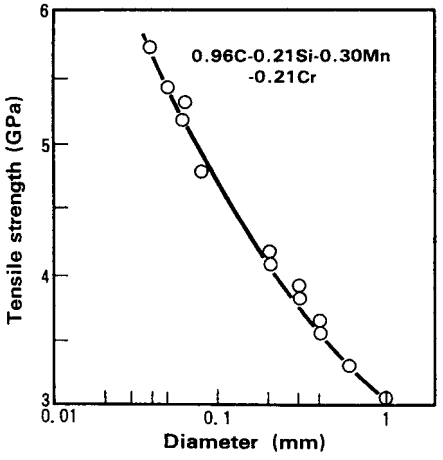

Fig. 15.8 Tensile strength as a function of wire diameter for patented and drawn pearlitic hypereutectoid steel wires. From Tarui et al., Ref 15.23

applications such as tire cord, conveyors, hoses, and bridge cables (Ref 15.23, 15.25).

The heat treatment that produces the starting microstructure for wire production is termed *patenting,* after a patented discovery by James Horsfall, Birmingham, England, in 1854 that made steel rod easier to draw (Ref 15.26). Patenting consists of heating to austenite and continuous cooling or isothermal holding to produce a uniform fine pearlite microstructure. Figure 15.10 shows an isothermal transformation diagram for eutectoid steel and the transformation temperature range to produce the desired fine pearlite microstructure for wire drawing (Ref 15.27). The

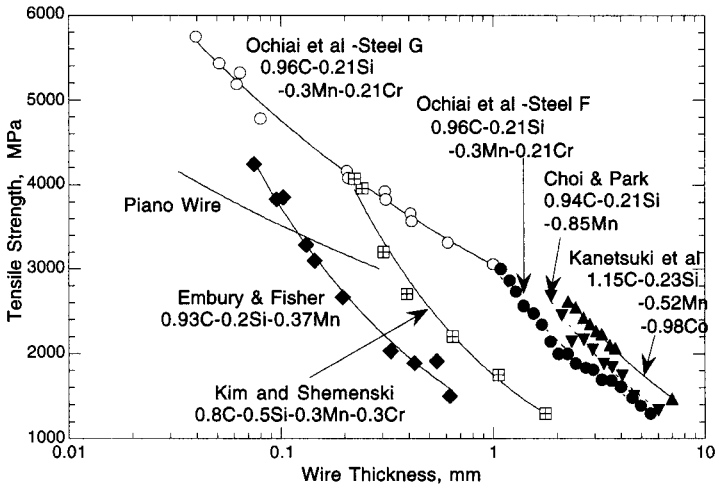

Fig. 15.9 Tensile strength as a function of wire diameter for patented and drawn wires in steels with pearlitic microstructures. From Lesuer et al., Ref 15.24. References to the investigations noted are given in Ref 15.24.

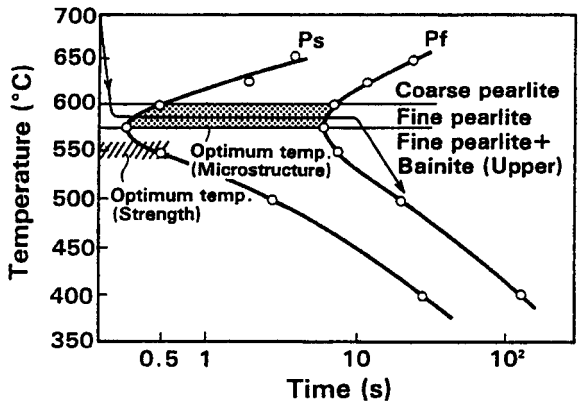

Fig. 15.10 Isothermal time-transformation diagram showing transformation temperature range for production of fine pearlite by patenting heat treatment. From Paris, Ref 15.27

microstructures, strengths, and ductilities of a hypereutectoid steel are shown as a function of transformation temperature in Fig. 15.11. Bainitic microstructures were found to be sensitive to delamination after drawing and, therefore, fine pearlite with a tensile strength of 1500 MPa (220 ksi) was found to be the most suitable starting microstructure for high-strength wire drawing (Ref 15.23).

Patenting may be applied to hot-rolled rod at the start of wire drawing or to cold-drawn wire as an intermediate heat treatment prior to further wire drawing. Fine pearlite has been traditionally produced in rods or wire isothermally transformed in molten lead baths, but alternative processing has been developed to produce good pearlitic microstructures directly after hot rolling to rod in high-speed bar mills (Ref 15.28, 15.29). The latter processing, first commercially applied in 1964, is copyrighted as the Stelmor process, and by 2003, 240 Stelmor process lines had been installed throughout the world. Stelmor processing consists of water cooling hot-rolled rod to a predetermined temperature, typically between 750 and 959 °C (1380 and 1740 °F), forming the rod into rings on a laying head, and fan air cooling the overlapping rings on a continuously moving conveyor. Cooling rates are adjusted to produce desired microstructures in various grades of steels, and after transformation, the rods are coiled for storage and further processing.

Wire Drawing Deformation of Pearlite for High-Strength Steel Wire

Fully pearlitic microstructures are highly deformable under wire drawing conditions. As strain increases, in longitudinal sections the lamellar structure of pearlite aligns itself parallel to the longitudinal wire axis (Ref 15.30), and in transverse sections the pearlitic structure becomes wavy

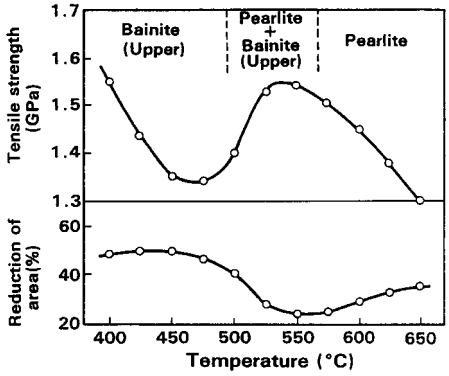

Fig. 15.11 Tensile strength and reduction of area as a function of transformation temperature and microstructure in patented hypereutectoid steels. From Tarui et al., Ref 15.23

and the lamellae within colonies are substantially curved (Ref 15.31). A ⟨110⟩ body-centered-cubic wire texture develops in the ferrite. The combination of closely spaced ductile ferrite and high-strength cementite lamellae makes possible exponential increases of strain hardening as a function of strain, in contrast to the linear increases with strain in ferritic iron wire without cementite (Ref 15.32). Although cementite is potentially brittle, in pearlitic structures the fracture resistance of cementite is a function of lamellae thickness. In coarse pearlite, cementite is brittle, but in microstructures where the interlamellar spacing is 0.10 μm or less, cementite has been shown to be partially or fully plastic (Ref 15.32).

The cementite lamellae of pearlite undergo dramatic changes during high-strain wire drawing (Ref 15.31–15.36). With increasing strain, the cementite lamellae become thinner, and both homogeneous bending and fragmentation of cementite lamellae may occur. In addition to slip deformation of the ferrite and cementite, localized shear band formation through the pearlite lamellae is another observed deformation mechanism. Cementite lamellae have been found to dissolve partially or completely at high strain deformation, and atom probe studies show that the carbon content of cementite decreases, and that of ferrite substantially increases, with the carbon apparently dissolved in the dislocation substructure of the ferrite. The carbon in solution in the ferrite then contributes to dynamic strain aging or to strain aging if wire is given subsequent low-temperature heat treatments.

Fracture Mechanisms of Patented and Drawn Steel Wire

As noted, fully pearlitic microstructures are capable of intensive wire drawing deformation. However, the severe deformation may result in unique types of failure. One type of fracture develops internally in response to hydrostatic tensile stresses that develop in the centers of wires during drawing (Ref 15.37). In plane longitudinal sections through damaged lengths of wire the cracks appear v-shaped, leading to the term *chevron cracking* to describe this type of fracture. The cracks are in fact axisymmetric, and when a wire breaks, the fracture surface appears conical, a fracture appearance termed *cuppy fracture* in the wire industry. The internal center cracking also leads to the term *centerline bursting* for this phenomenon. Similar stress states to those in wires also create centerline, v-shaped cracks in extruded rods, and examples of such cracking, also typical of centerline cracking in wire, are shown in Fig. 15.12 (Ref 15.37). In wires, nondeforming microstructural features in the centers of wires, such as inclusions, grain boundary cementite, or residual centerline segregation that provides sufficient hardenablity for martensite formation, may be associated with initiation of chevron cracking. Therefore, consid-

erable attention must be paid to steel quality and primary steel processing (Ref 15.38, 15.39).

Control of wire drawing parameters may also minimize chevron cracking (Ref 15.37). A parameter Δ defines the deformation zone geometry for the generation of hydrostatic tensile stresses as the ratio of the mean diameter of the work to the contact length between the die and the work and is in turn related to reduction ratio and die angle. High values of Δ increase susceptibility to chevron cracking and are produced by lower reductions and high die angles.

Some high-strength patented and drawn wires are twisted into cables and bunches. As a result, not only must the wire have high tensile strength, it also must have good torsional strength and good resistance to shear stresses. Figure 15.13 shows the longitudinal and transverse orientation

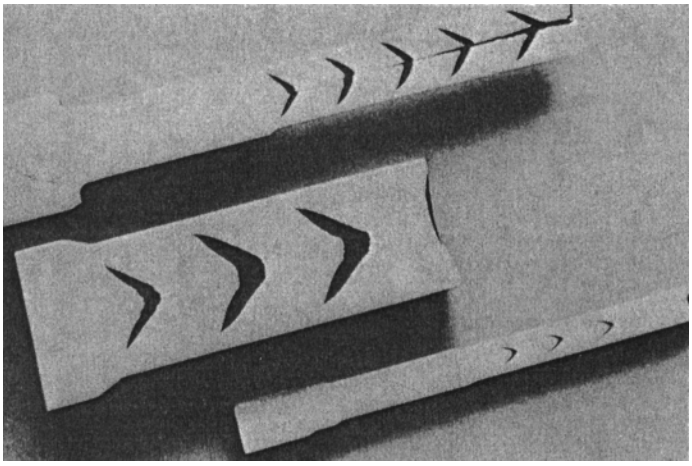

Fig. 15.12 Centerline bursting or chevron cracks, similar to those that form under certain conditions in drawn patented wires, in extruded steel rods. From D.J. Blickwede as reproduced in Hosford and Caddell, Ref 15.37

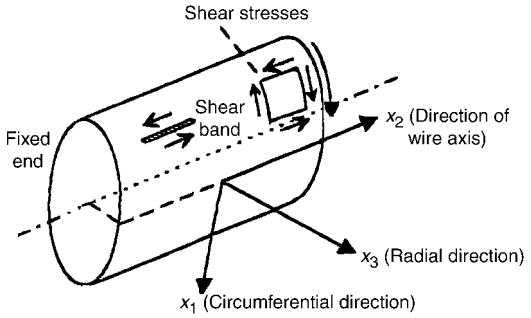

Fig. 15.13 Schematic diagram of a length of wire showing orientations of shear stresses produced during torsion and a longitudinal shear band that leads to delamination fracture of patented and drawn pearlitic wires. From Lefever et al., Ref 15.40

of shear stresses that develop in a torsion tested wire (Ref 15.40). For wires with fine, uniformly deformed pearlitic microstructures and good surface condition, after a significant number of applied torsional twists, smooth, flat shear fractures develop on transverse wire surfaces. However, under some conditions, surface shear bands develop in response to the longitudinal shear stresses, and these bands eventually nucleate shear cracks characterized by joining of fine microvoids. With increased twisting, the longitudinal cracks assume a helical or spiral orientation, as shown schematically in Fig. 15.14. The spiral crack is labeled "secondary fracture," and a transverse shear fracture surface, also shown, is labeled "primary fracture."

The longitudinal cracking or splitting along the wire surface during torsion testing is referred to as *delamination* (Ref 15.40, 15.42). Once initiated, compressive stresses close the spiraling delamination crack, and the wire may undergo further twisting despite significant damage. Good surface conditions are important to prevent delamination, but microstructural factors must also be optimized. Tarui et al. emphasize that fine as-patented pearlite is the key to high-strength wire with good delamination resistance and that upper bainite formed at low transformation temperatures lowers delamination resistance (Ref 15.23, 15.43). Strengthening by chromium and vanadium additions and higher carbon content were found to be more effective than increased drawing reduction in producing strength and while maintaining good delamination resistance. Tarui et al. also show that silicon and chromium additions to patented and drawn microstructures suppress spheroidization of pearlitic cementite and the attendant strength loss during hot dip galvanizing at 450 °C (840 °F). Nam and Bae confirm that coarse pearlite lowers delamination resistance and note that globular cementite particles contribute to the inititation of delamination (Ref 15.43). Low-temperature aging or stress relief treatments of patented and drawn wires also result in reduced delamination resistance (Ref 15.42).

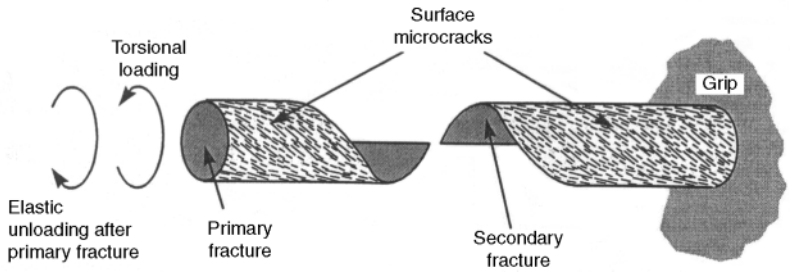

Fig. 15.14 Schematic diagram of torsion-tested wire in which a primary transverse shear fracture and a spiral delamination fracture (labeled "secondary fracture") have developed. From Goes et al., Ref 15.41

REFERENCES

15.1 T. Gladman, I.D. McIvor, and F.B. Pickering, Some Aspects of the Structure-Property Relationships in High-Carbon Ferrite-Pearlite Steels, *Journal of the Iron and Steel Institute,* Vol 210, 1972, p 916–930

15.2 J.M. Hyzak and I.M. Bernstein, The Role of Microstructure on the Strength and Toughness of Fully Pearlitic Steels, *Metallurgical Transactions A,* Vol 7A, 1976, p 1217–1224

15.3 Y.-J. Park and I.M. Bernstein, Mechanisms of Cleavage Fracture in Fully Pearlitic 1080 Rail Steel, *Rail Steels—Developments, Processing and Use,* STP 644, ASTM, 1978, p 287–302

15.4 *Rail Steels—Developments, Processing, and Use,* D.H. Stone and G.G. Knupp, Ed., STP 644, ASTM, 1978

15.5 *Rail Steels—Developments, Manufacturing and Performance,* B.L. Bramfit, R.K. Steele, and J.H. Martens, Ed., ISS, Warrendale, PA 1993

15.6 *Rail Steels for the 21st Century,* B.L. Bramfit, R.K. Steele, and J.H. Martens, Ed., ISS, Warrendale, PA, 1995

15.7 G.G. Knupp, W.H. Chidley, J.L. Giove, H.H. Hartman, G.F. Morris, and C.W. Taylor, A Review of the Manufacture, Processing, and Use of Rail Steels in North America—A Report of AISI Technical Subcommitee on Rails and Accessories, in Ref 15.4, p 7–20

15.8 R.K. Steele, "A Perspective Review of Rail Behavior at the Facility for Accelerated Service Testing," Report FRA/TTC-81/07, U.S. Department of Transportation, Federal Railroad Administration, Washington, D.C., 1981

15.9 E.L. Brown and G. Krauss, unpublished research, Colorado School of Mines, 1982

15.10 A. Kapoor, Wear by Plastic Ratchetting, *Wear,* Vol 212, 1997, p 119–130

15.11 P. Clayton and D. Danks, Effect of Interlamellar Spacing on the Wear Resistance of Eutectoid Steels under Rolling/Sliding Conditions, *Wear,* Vol 135, 1990, p 369–387

15.12 B.L. George, J.B. McDonald, and F.W. Kokoska, Residual Stresses in Off-Line Head Hardened Steels, in Ref 15.5, p 79–91

15.13 B.L. Bramfit, Advanced In-Line Head Hardening of Rail, in Ref 15.6, p 23–29

15.14 G.K. Bouse, I.M. Bernstein, and D.H. Stone, Role of Alloying and Microstructure on the Strength and Toughness of Experimental Rail Steels, in Ref 15.4, p 145–166

15.15 S. Marich and P. Curcio, Development of High-Strength Alloyed Rail Steels Suitable for Heavy Duty Applications, in Ref 15.4, p 167–211

15.16 Y.E. Smith and F.B. Fletcher, Alloy Steels for High-Strength, As-Rolled Rails, in Ref 15.4, p 212–232

15.17 K. Han, T.D. Mottishaw, G.D.W. Smith, D.V. Edmonds, and A.G. Stacey, Effects of Vanadium Additions on Microstructure and Hardness of Hypereutectoid Pearlitic Steels, *Materials Science and Engineering A,* Vol 190, 1995, p 207–214

15.18 K. Han, G.D.W. Smith, and D.V. Edmonds, Pearlite Phase Transformation in Si and V Steel, *Metallurgical and Materials Transactions A,* Vol 26A, 1995, p 1617–1631

15.19 M. Ueda, K. Uchino, and T. Senuma, Effects of Carbon Content on Wear Property in Pearlitic Steels, *Thermec 2003,* T. Chandra, J.M. Torralba, and T. Sakai, Ed., Part 2, Trans Tech Publications, 2003, p 1175–1180

15.20 J. Kalousek and A.E. Bethune, Rail Wear under Heavy Traffic Conditions, in Ref 15.4, p 63–79

15.21 D.H. Stone and R.K. Steele, The Effect of Mechanical Properties upon the Performance of Railroad Rails, in Ref 15.4, p 21–62

15.22 R.K. Steele and M.W. Joerms, Plastic Deformation and Its Relationship to Rail Performance, in Ref 15.6, p 79–91

15.23 T. Tarui, T. Takahashi, H. Tashiro, and S. Nishida, Metallurgical Design of Ultra High Strength Steel Wires for Bridge Cable and Tire Cord, *Metallurgy, Processing and Applications of Metal Wires,* H.G. Paris and D.K. Kim, TMS, Warrendale, PA, 1996, p 87–96

15.24 D.R. Lesuer, C.K. Syn, O.D. Sherby, and D.K. Kim, Processing and Mechanical Behavior of Hypereutectoid Steeel Wires, *Metallurgy, Processing and Applications of Metal Wires,* H.G. Paris and D.K. Kim, TMS, Warrendale, PA, 1996, p 109–121

15.25 O. Arkens, Steel Is Still King in Tyres, *Metallurgy, Processing and Applications of Metal Wires,* H.G. Paris and D.K. Kim, TMS, Warrendale, PA, 1996, p 75–86

15.26 *Steel Wire Handbook,* Vol 2, A.B. Dove, Ed., The Wire Association, Branford Connecticut, 1969

15.27 H. Paris, Metallurgy, Processing and Applications of Metal Wires—A Review, *Metallurgy, Processing and Applications of Metal Wires,* H.G. Paris and D.K. Kim, Ed., TMS, Warrendale, PA, 1996, p 3–15

15.28 *Ferrous Wire*—Vol 1, Chapter 5A, Controlled Cooling of Wire Rod, *Wire Handbook*

15.29 P.L. Keyser and B.V. Kiefer, STELMOR In-Line Controlled Cooling Process for High Speed Rod Mills, *Materials Solution Conference,* ASM International, 1997

15.30 J.D. Embury and R.M. Fisher, The Structure and Properties of Drawn Pearlite, *Acta Metallurgica,* Vol 14, 1966, p 147

15.31 G. Langford, A Study of the Deformation of Patented Steel Wire, *Metallurgical Transactions,* Vol 1, 1970, p 465–477

15.32 G. Langford, Deformation of Pearlite, *Metallurgical Transactions A,* Vol 8A, 1977, p 861–875

15.33 M. Zelin, Microstructure Evolution in Pearlitic Steels during Wire Drawing, *Acta Materialia,* Vol 50, 2002, p 4431–4447

15.34 M.H. Hong, W.T. Reynolds, Jr., T. Tarui, and K. Hono, Atom Probe and Transmission Electron Microscopy Investigations of Heavily Drawn Pearlitic Steel Wire, *Metallurgical and Materials Transactions A,* Vol 30A, 1999, p 717–727

15.35 S. Tagashira , K. Sakai, T. Furuhara, and T. Maki, Deformation Microstructure and Tensile Strength of Cold Rolled Pearlitic Steel Sheets, *ISIJ International,* Vol 40, 2000, p 1149–1156

15.36 M. Umemoto, Y. Todaka, and K. Tsuchiya, Mechanical Properties of Cementite and Fabrication of Artificial Pearlite, *Materials Science Forum,* Vol 426–432, 2003, p 859–864

15.37 W.F. Hosford and R.M. Caddell, *Metal Forming: Mechanics and Metallurgy,* PTR Prentice Hall, Englewood Cliffs, NJ, 1993

15.38 I. Chakrabarti, S. Sarkar, M.D. Maheshwari, U.K. Chaturvedi, and T. Mukherjee, Process Enhancements to Improve Drawability of Wire Rods, *Tata Search,* Vol 1, 2004, p 232–240

15.39 S.K. Choudhary, M.N. Poddar, B.K. Jha, and H.J. Billimoria, Inclusion Characteristics of High Carbon Steel for Wire Drawing, *Tata Search,* Vol 1, 2004, p 241–248

15.40 I. Lefever, U.D. D'Haene, W. Van Raemdonck, E. Aernoudt, P. Van Houtte and J. Gil Sevillano, Modeling of the Delamination of High Strength Steel Wire, *Wire Journal International,* November 1998

15.41 B. Goes, A. Martin-Meizoso, J. Gil-Sevillano, I. Lefever, and E. Aernoudt, Fragmentation of As-Drawn Pearlitic Steel Wires during Torsion Tests, *Engineering Fracture Mechanics,* Vol 60 (No. 3), 1998, p 255–272

15.42 W. Van Raemdonck, I. Lefever, and U. D'Haene, Torsions Tests as a Tool for High Strength Wire Evaluation, *Wire Journal International,* Vol 6, 1994, p 68

15.43 W.J. Nam and C.M. Bae, The Effect of Interlamellar Spacing on the Delamination Behavior of Severely Drawn Pearlitic Steel Wire, in *Metallurgy, Processing and Applications of Metal Wires,* H.G. Paris and D.K. Kim, Ed., TMS, Warrendale, PA, 1996, p 243–250

ASM International is the society for materials engineers and scientists, a worldwide network dedicated to advancing industry, technology, and applications of metals and materials.

ASM International, Materials Park, Ohio, USA
www.asminternational.org

Publication title	Product code
Steels: Processing, Structure, and Performance	05140G

To order products from ASM International:

Online Visit www.asminternational.org/bookstore

Telephone 1-800-336-5152 (US) or 1-440-338-5151 (Outside US)

Fax 1-440-338-4634

Mail Customer Service, ASM International
9639 Kinsman Rd, Materials Park, Ohio 44073, USA

Email CustomerService@asminternational.org

In Europe American Technical Publishers Ltd.
27-29 Knowl Piece, Wilbury Way, Hitchin Hertfordshire SG4 0SX, United Kingdom
Telephone: 01462 437933 (account holders), 01462 431525 (credit card)
www.ameritech.co.uk

In Japan Neutrino Inc.
Takahashi Bldg., 44-3 Fuda 1-chome, Chofu-Shi, Tokyo 182 Japan
Telephone: 81 (0) 424 84 5550